energies

MDPI

Article

Permeability and Mechanical Response of Granite after Thermal and CO_2 Bearing Fluid Hydro-Chemical Stimulation

Rong-Chen Tong [1,2], He-Juan Liu [1,2,*], Yu-Jia Song [1,2], Li-Huan Xie [1,2] and Sheng-Nan Ban [1,2]

[1] State Key Laboratory of Geomechanics and Geotechnical Engineering, Institute of Rock and Soil Mechanics, Chinese Academy of Sciences, Wuhan 430071, China
[2] University of Chinese Academy of Sciences, Beijing 100049, China
* Correspondence: hjliu@whrsm.ac.cn

Abstract: The large scale extraction of geothermal energy can reduce CO_2 emissions. For hot dry rocks, the key to successful utilization depends on the efficiency of reservoir reconstruction. The chemical and thermal stimulation methods are always used in geothermal reservoir reconstruction except in hydraulic fracturing with high fluid injection pressure, which is believed to reduce the seismic hazard by applying before the high-pressure hydraulic fracturing stimulation. However, at the laboratory scale, there are still very limited experimental studies illustrating the combined effects of chemical and thermal stimulation on the permeability and mechanical properties of granite, which is regarded as the main type of hot dry rock. In this paper, comparative stimulation experiments were carried out, including thermal/cold stimulation, CO_2 bearing solution hydro-chemical stimulation, combined thermal and CO_2 bearing fluid stimulation. By means of nuclear magnetic resonance analysis, permeability test and triaxial compression test, the changes of the micro-structure, permeability and mechanical properties of granite under various stimulation conditions were analyzed. The experimental results show that, compared with the single thermal stimulation and CO_2 bearing fluid hydro-chemical stimulation, the superposition effect of thermal and CO_2 bearing fluid hydro-chemical stimulation can increase the number of micro-fractures in granite more effectively, thus increasing the permeability, while the elastic modulus and compressive strength decrease. Moreover, the cooling mode on the granite also has a certain influence on the stimulation effect. After water-cooling on the heated granite (300 °C), combined with the CO_2 bearing fluid stimulation (240 °C, 20 MPa), the permeability of granite is the highest, increasing by 17 times that of the initial state, and the porosity also increases by 144.4%, while the elastic modulus and compressive strength decrease by 14.3% and 18.4%, respectively. This implies that the deterioration of mechanical properties due to the micro-fractures increased by the thermal and chemical stimulation can enhance the fluid conductivity and heat extraction of granite. The methods in this paper can provide a reference for the combined application of thermal and chemical stimulation technology in artificial reservoir reconstruction of hot dry rocks.

Keywords: granite; thermal-cold stimulation; permeability; mechanical properties; CO_2 bearing solution

Citation: Tong, R.-C.; Liu, H.-J.; Song, Y.-J.; Xie, L.-H.; Ban, S.-N. Permeability and Mechanical Response of Granite after Thermal and CO_2 Bearing Fluid Hydro-Chemical Stimulation. *Energies* **2022**, *15*, 8280. https://doi.org/10.3390/en15218280

Academic Editors: Fangtian Wang, Wai Li, Lidong Mi and Meng Meng

Received: 16 September 2022
Accepted: 1 November 2022
Published: 5 November 2022

1. Introduction

Enhanced geothermal system (EGS) is applied in the hot dry rocks, which is significant in increasing the fluid flow pathways and heat exchange capacity after creating the artificial fracture network, making it more efficient to extract the geothermal energy in the granite type of hot dry rocks [1–3]. Except hydraulic fracturing, which is the main means of reservoir reconstruction in granite [4], the supercritical CO_2 fracturing technology is often applied, which can also store the CO_2 in the formation, decreasing the CO_2 emission in the atmosphere [5,6]. These strong stimulation methods, including hydraulic fracturing and supercritical CO_2 fracturing at high fluid injection pressure, increase the risk of induced micro-seismic events and even destructive earthquakes [7–11]. In EGS engineering, the

poor hydraulic connection between production wells/injection wells is often encountered due to the improper fracture network in granite by the strong fracturing stimulation. In order to expand the fracture network and increase the permeability of the granite, some supplemented stimulation methods are usually used before the strong fracturing technology [12,13]. It was believed that the chemical or thermal stimulation means, especially the combined effects of the chemical or thermal stimulation, can reduce the strength of fracturing technology, thereby reducing the earthquake risk caused by high-pressure hydraulic stimulation. However, at the laboratory scale, there is no systematic understanding of the effect of combined chemical-thermal stimulation on the micro-structure permeability and mechanical properties of granite.

In EGS engineering, the thermal stimulation method has been widely used by continuously injecting low-temperature fluid into the high-temperature rock mass. Micro-fractures in rock mass will constantly expand under the action of thermal shock [14]. It is of great practical significance to study the mechanical and permeability characteristics of granite with high temperature after thermal shock. The microscopic characteristics of granite after high-temperature heating were studied and it was found that thermal damage will lead to changes in the internal micro-structure of rock mass, which will then affect the permeability characteristics of granite [14–16]. Alm et al. [17] carried out experiments on the mechanical characteristics of granite after thermal treatment at different temperatures and discussed the evolution of the micro-fractures under the action of temperature. Kumari et al. [18] studied the fracture characteristics of granite under different cooling rates and the impact of thermal shock effect caused by rapid cooling on the micro-structure of granite, pointing out that thermal shock can lead to the generation of micro-fractures. Brotóns et al. [19] showed that different cooling methods on the rocks at high-temperature cause different temperature gradients and that the physical and mechanical properties of rocks are affected at different levels. The mechanical strength weakening caused by water cooling is greater than that caused by natural cooling. Zhang et al. [20] studied the changes of seepage characteristics, P-wave velocity, elastic modulus and compressive strength of granite treated with high temperature heating and water cooling. The results showed that the generation of new fractures caused by thermal treatments is the main reason for the deterioration of the rock's physical and mechanical properties.

Chemical stimulation is often used to enhance the reservoir permeability in oil and gas engineering and geothermal engineering. Various chemical solutions (e.g., mud acid, NTA solution, CO_2 solution) are often injected into the reservoir near the well at an injection pressure lower than the formation rupture pressure. By chemical dissolution of minerals, such as siliceous and calcareous, the scaling of the well bore or the blockage near the well can be solved [21–27]. Some scholars have studied the interaction between CO_2-water-rock through hydrothermal experiments [28–31]. The research results showed that CO_2-bearing fluid has the ability to dissolve minerals such as calcite, feldspar and quartz in sandstone, which leads to the expansion of rock pores and the destruction of cements, decreasing the mechanical strength of rock significantly [30,31]. Liu et al. [32] used mud acid stimulants with different concentrations and alkaline stimulants (e.g., $NaHCO_3$ solution and NaOH solution) to conduct chemical corrosion experiments on granite and discovered that both of them increase the dissolution of mineral particles in granite, thus the micro-structure, porosity and permeability are varied at different levels. Miao et al. [33] studied the relationship between mechanical properties of granite and pH of solution through experiments in an acidic environment. The research results showed that elastic modulus, tensile strength, uniaxial compressive strength, triaxial compressive strength and other parameters all reduced with the decrease of pH value. However, in the geological environment of granite type of hot dry rocks with high temperature and pressure, the reaction rate of common chemical stimulation fluid with rock mass minerals is too fast, and only the rock mass near the injection well is dissolved, which is consumed after slightly entering the reservoir. The ideal penetration distance cannot be maintained [34]. In view of the above problems, the use of CO_2 as a stimulus has been proposed [34,35].

In the CO_2 bearing solution, the mineral quartz in granite will dissolve, and the minerals such as potassium feldspar, albite and calcium feldspar will react with the weak carbonic acid [36–40]. Under the confining pressure of 30 MPa and the temperature of 100, 200 and 300 °C, the triaxial compressive strength of granite decreased by 3.83%, 2.59% and 1.44%, respectively, after reacting with CO_2 bearing aqueous solution for six months [41].

In this paper, thermal stimulation and CO_2 solution stimulation are carried out on granite. On one hand, it can illustrate whether CO_2 bearing solution stimulant is helpful for physical property transformation of reservoir. On the other hand, it also helps to clarify how the mechanical properties of granite will be affected under the combined stimulation methods before the strong fracturing technology that may cause the seismic risk in the hot dry rocks. Therefore, a set of comparative experiments were carried out in this paper, including thermal stimulation, CO_2 aqueous solution stimulation, and combined stimulation of thermal and CO_2 bearing solution. Through nuclear magnetic resonance analysis, permeability test, triaxial compression test and other means. The changes of microscopic pore-fracture structure, permeability characteristics, and the mechanical properties of granite under different stimulation methods were analyzed.

2. Materials and Methods

2.1. Sample Preparation

The granite was collected from the Triassic Sanguliu pluton located in the Liaodong area, more details can be seen in our previous work [2]. It has coarse grain structure, and inter-granular cracks and intracrystalline cracks developed (Figure 1). The mineralogy of granite includes potassium feldspar, albite, quartz, amphibole, etc. (see Table 1). The granite was cut into a cylindrical specimen with a height of 50 mm and a diameter of 25 mm (Figure 2), and the P-wave velocity is in the range of 3700 m/s and 4000 m/s.

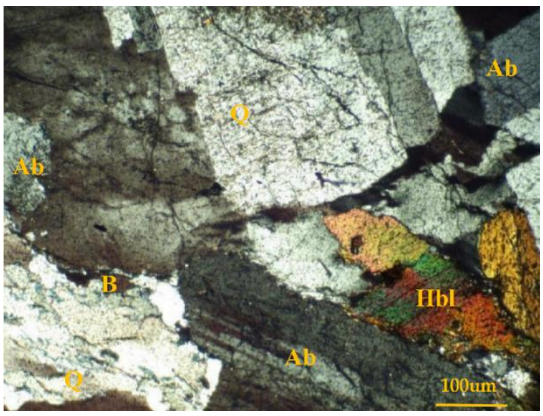

Figure 1. Micro cracks developed in the granite observed by the optical microscopy (Ab: albite, Q: quartz, Hbl: hornblende, B: biotite).

Figure 2. Granite samples in the Sanguliu pluton of the Liaodong area.

Table 1. Mineral composition of granite used in the experiments.

Potassium Feldspar	Albite	Quartz	Biotite	Hornblende	Clinochlore
30.7%	27.3%	21.8%	14.2%	4.4%	1.6%

2.2. Experimental Conditions Set-Up

Four groups of comparison experiment samples were set, namely (1) original samples group (S0-1, S0-2, S0-3), (2) pure thermal stimulation group (S-1, S-2), (3) pure CO_2 bearing solution stimulation group (S-3, S-4), (4) combined stimulation of thermal and CO_2 bearing solution group (S-5, S-6, S-7 and S-8). The specific experimental conditions of each granite sample are shown in Table 2.

Table 2. Experimental conditions in the comparative stimulation.

Group	Number	Heat Treatment Conditions	Cooling Mode	Water-Rock Reaction Conditions	Reaction Time (d)
Original sample	S0-1	–	–	–	–
	S0-2				
	S0-3				
Thermal-cold stimulation	S-1	300 °C, 4 h	Natural cooling	–	–
	S-2	300 °C, 4 h	Water cooling	–	–
CO_2 stimulation	S-3	–	–	240 °C, 20 MPa	7
	S-4	–	–	240 °C, 20 MPa	14
Thermal + chemical stimulation	S-5	300 °C, 4 h	Natural cooling	240 °C, 20 MPa	7
	S-6	300 °C, 4 h	Natural cooling	240 °C, 20 MPa	14
	S-7	300 °C, 4 h	Water cooling	240 °C, 20 MPa	7
	S-8	300 °C, 4 h	Water cooling	240 °C, 20 MPa	14

In the process of thermal stimulation, in order to study the difference of the stimulation effect of different cooling rates on the sample, we set two cooling methods: natural cooling and water cooling. The granite samples (S-1, S-2, S-5, S-6, S-7, S-8) were heated to 300 °C, which fits the definition of hot dry rocks from the temperature point of view (>150 °C), and it was observed that microcracks can occur in granite above 300 °C. All samples were kept for 4 h to ensure a uniform heating inside the sample, at a heating rate of 5 °C/min by an SX2 muffle furnace produced by Subo Instrument Co., Ltd (Shaoxing, China). Then, the granite samples were cooled at room temperature by natural cooling (S-1, S-5, S-6) and water cooling (S-2, S-7, S-8), respectively. For the water cooling process, the sample was removed from the muffle furnace and immediately soaked in a container containing 10 L water at room temperature, and the granite sample was quickly removed from the water every 5 s to measure the temperature decrease by infrared thermometer and then was soaked in the water repeatedly until the rock sample reached room temperature.

In the CO_2 bearing solution hydro-chemical stimulation, where the test system with high temperature and high pressure was used (Figure 3), the test system is mainly composed of three parts: (1) The CO_2 injection part, which is composed of a CO_2 cylinder and the ISCO pressure pump, is used to continuously provide CO_2 gas and steady pressure during the reaction; (2) The reaction vessel, the main body of which is a high temperature and high pressure reaction kettle, is equipped with heating and insulation function, which can provide a stable and safe reaction environment and conditions for the CO_2-water-rock reaction, with an inner volume size of ϕ 75 mm × 160 mm, the maximum working pressure of 40 MPa and the maximum working temperature of 350 °C; (3) The automatic monitoring part can record and regulate the temperature and pressure in the reaction kettle in real time.

The specific experiment was as follows: S-3, S-5 and S-7 were placed in the reaction kettle, and 900 mL deionized water was added to the reaction kettle to ensure that the rock sample was completely soaked. After the reactor was completely sealed, it was heated until the temperature reached 240 °C, and CO_2 was also added into the reactor until the pressure reached 20 MPa. The reaction time was 7 days. S-4, S-6 and S-8 were also treated in the above way, but their reaction time was 14 days.

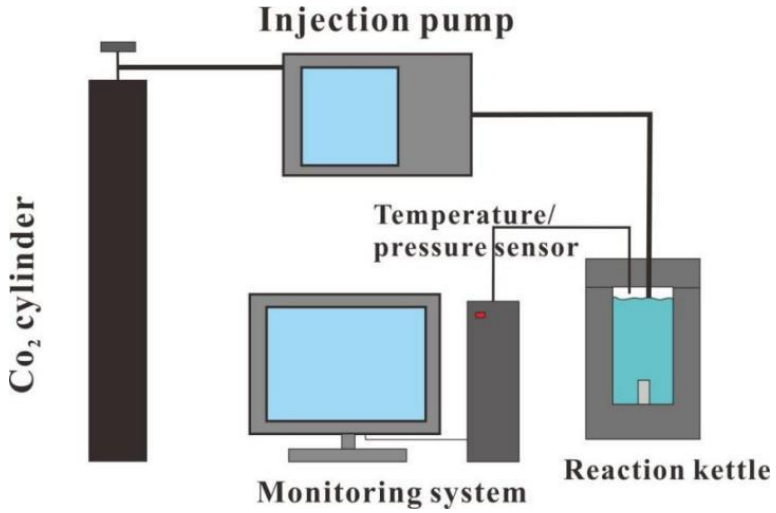

Figure 3. The fluid-rock reaction test system with high temperature and high pressure.

After the experiments, nuclear magnetic resonance analysis, permeability test and conventional triaxial compression test were carried out on all samples for comparison and analysis in the changes of microscopic pore-fracture structure, permeability and mechanical properties of granite.

2.3. Test and Analysis Methods

2.3.1. Nuclear Magnetic Analysis

MacroMR12–150 h nuclear magnetic resonance (NMR) analysis system, produced by NIUMAG Analytical Instrument Co., Ltd. (Suzhou China), was used to analyze the microscopic pore-fracture structure of the granite samples. The nuclear magnetic resonance test and analysis system can apply an external magnetic field to the sample, and through the inversion of the free induction attenuation signal, the T_2 spectra of the transverse relaxation time of water particles in the pores or fractures in the rocks, can be measured so that it can quantitatively analyze the microscopic pore-fracture structure of granite [42–44].

When the rock is saturated with water, its relaxation time can be calculated by Equation (1) [42]:

$$\frac{1}{T_2} = \rho_2 \left(\frac{S}{V} \right) \tag{1}$$

where, T_2 is the relaxation time, ms; S is the pore surface area, m^2; V is the pore volume, m^3; ρ_2 is the relaxation constant of rock surface, m/ms. If the rock pores are simplified into a spherical or cylindrical shape for analysis, Equation (1) can be further simplified into Equation (2):

$$\frac{1}{T_2} = \frac{\rho_2}{r} F_S \tag{2}$$

where r is the pore radius, m; F_s is the geometry factor: F_s = 3 for spherical pores; F_s = 2 for columnar pores. In fact, the pore shapes of granite are complex. Therefore, it is impractical to determine the value of F_s and ρ_2, respectively. However, according to engineering practice, for granite the product of F_s and ρ_2 is relatively fixed and can be taken as 1×10^{-8} m/ms [45]. The T_2 distribution can reflect the pore size and distribution in the granite

sample, the relaxation time reflects the pore size, the peak area reflects the pore volume and the amplitude reflects the number of pores in the corresponding pore size.

Through the calibration of standard samples, the conversion relationship between NMR signal value and actual porosity can be obtained, and the relationship is as follows:

$$Y = 2.44 \times 10^5 X + 2000 \quad (3)$$

where Y is the nuclear magnetic signal value of the rock sample, X is the total porosity of the rock sample, and R^2 of the fitting result is 0.995. After conducting NMR tests on the rock samples, the nuclear magnetic signal value can be substituted into Equation (3) to further calculate the total porosity of the rock samples.

2.3.2. Transient Pulse Method

In this paper, the transient pulse method was used to measure the permeability of granite before and after the stimulation experiment by the equation as follows:

$$k = \frac{V_u V_d}{V_u + V_d} \frac{\gamma \mu L}{A \Delta t} ln \frac{\Delta P}{\Delta P_0} \quad (4)$$

where, V_u and V_d are the volumes of the upstream and downstream pressure chambers, which are 0.00612 L and 0.00451 L, respectively. μ is the dynamic viscosity coefficient of nitrogen that we used and set as 1.75×10^{-5} Pa·s. γ is the compression coefficient and set as 2×10^{-6} Pa^{-1}; L and A are the length and cross-sectional area of the sample; Δt is the test time, s; ΔP_0 and ΔP are the initial pressure difference and real-time pressure difference, respectively, and ΔP_0 = 0.5 MPa.

2.3.3. Triaxial Compression Test

An MTS815.03 electro-hydraulic servo triaxial testing machine was used to evaluate the mechanical properties of four groups of granite samples. The high-precision servo system and sensor ensured the accurate recording of load and deformation. The confining pressure of the test is set as 10 MPa, and the axial constant loading rate is 0.0005 mm/s. The elastic modulus and peak strength of the samples were obtained by the triaxial compression tests.

3. Results and Discussion

3.1. Changes of Micro-Structure and Permeability of Granite

3.1.1. T_2 Spectra and Distribution of Pore-Fracture

The T_2 spectra of each sample after the stimulation is shown in Figure 4 (only S0-1 is selected for comparison in the original sample group). On the basis of the Hodot classification system, according to the relationship between the pore diameter and T_2 relaxation time in Equation (2), the pore-fracture structure can be classified according to the T_2 relaxation time [46–49] (micro-pore, <1 ms; transition pore, 1–10 ms; mesopore, 10–100 ms; macro-pore/micro-fracture, >100 ms). According to existing studies [50–53], mesopores, macro-pores and micro-fractures contribute to most of the porosity and provide the main space and paths for gas and water flow. It is not difficult to see from Figure 4 that the T_2 spectra of each granite sample can be roughly divided into left and right peaks with T_2 = 10 ms as the dividing line. The left peak range basically includes micro-pores or micro-cracks (<1 ms) and transition pores or cracks (1–10 ms), while the right peak range basically includes mesopores (10–100 ms) and macro-pores/micro-fractures (>100 ms). In this paper, to simplify the above classification standards, the left peak range of T_2 spectra represents micro-cracks and the right peak range of T_2 spectra represents micro-fractures [54].

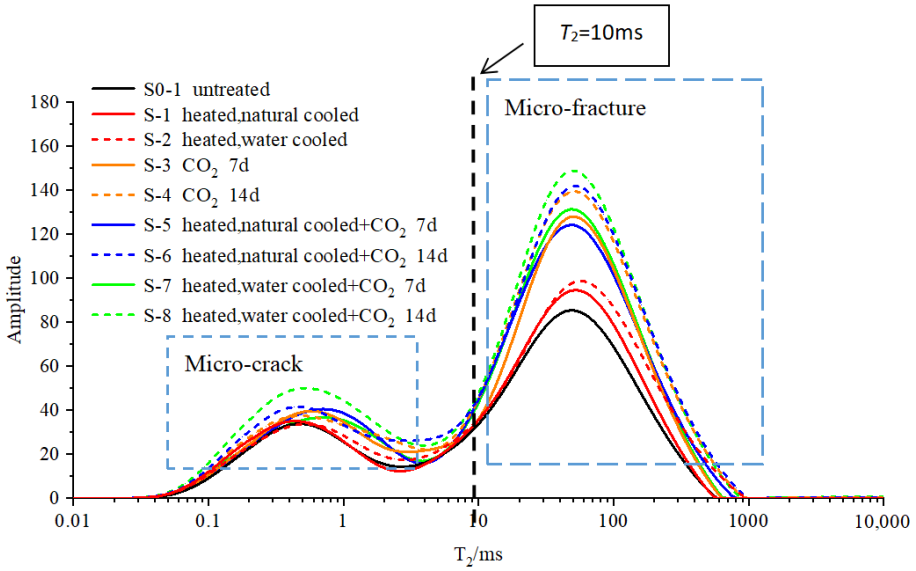

Figure 4. T_2 spectra of granite under the action of different stimulation.

As can be seen from Figure 4, the T_2 spectra of granite samples after either pure thermal treatment or CO_2-water-rock reaction at high temperature and pressure all show double peak characteristics, and the right peak is the dominant type. The effective signal is mainly concentrated between 0.01~10,000 ms, and the relaxation time corresponding to the left peak point of all T_2 spectra is in the range of 0.1~1 ms, while the relaxation time corresponding to the right peak point is in the range of 40~60 ms, indicating that the micro-fractures' distribution before and after the experiments is similar.

Figure 5 shows the areas of left and right peak, the total spectra area, and the proportions of left and right peak area of the T_2 spectra of each granite sample. The total spectral areas of the three original samples S0-1, S0-2 and S0-3 are 3977, 3910 and 4000, respectively. Because their values are very close, only S0-1 is selected as a representative sample to be shown in Figure 5. As shown in Figure 5a, comparing the T_2 spectra data of the original sample (S0-1) and the thermal stimulation group (S-1 and S-2), the total spectra areas are 3956.838, 4305.153 and 4683.729, respectively. It shows that the total spectra area of the sample increases to a certain extent after high temperature heating at 300 °C, and the total spectra area of the sample after water cooling further increases compared with the sample cooled at room temperature. Specifically, the spectra area of the left peak changes slightly, while the spectra area of the right peak increases significantly, which indicates that micro-cracks are not significantly affected, micro-fractures in the sample have obvious development and the number has increased.

Comparing the original sample group (S0-1) with the CO_2 stimulation group (S-3 and S-4), the total spectra areas of S-3 and S-4 are 5448.876 and 6198.318, respectively, indicating that the number of internal micro-fractures of the granite sample increases significantly after CO_2-water-rock reaction at high temperature and high pressure. The left peak area and the right peak area of the three increase respectively. It can be seen that the pores and fractures of different size are developed to a certain extent.

Through comparative analysis of the CO_2 stimulation group (S-3, S-4) and the combined stimulation group (S-5, S-6), the total spectra areas of S-3 and S-5 are 5448.578 and 5587.507, respectively. It can be seen that compared with the pure CO_2 bearing solution stimulation, the total pore or fracture volume of the sample after combined stimulation slightly increases, and the increases of macro-pores/micro-fractures are relatively more obvious. The total spectra areas of S-4 and S-6 are 6198.318 and 6404.335, respectively. It can be seen that with the extension from 7 d to 14 d of CO_2-water-rock reaction, the scheme of combined stimulation has more obvious advantages than that of pure CO_2 bearing solution stimulation, and the relative stimulation effect is better.

Comparing S-5, S-6, S-7 and S-8, the total spectra areas of S-5 and S-7 are 5587.507 and 5622.653, respectively, while the total spectra areas of S-6 and S-8 are 6404.335 and 6835.648, respectively. Compared with S-5, S-7 has a larger total spectra area and a larger total pore or fracture volume, in which the number of micro-pores does not change significantly, while the number of macro-pores/micro-fractures increases. Similarly, compared to S-6, S-8 has a more obvious increase in the total spectra area and a significant increase in the number of both micro-pores and macro-pores/micro-fractures, which indicates that, with the increase of CO_2-water-rock reaction time, the cooling mode after high-temperature heating has a more obvious impact on the final effect of superposition stimulation.

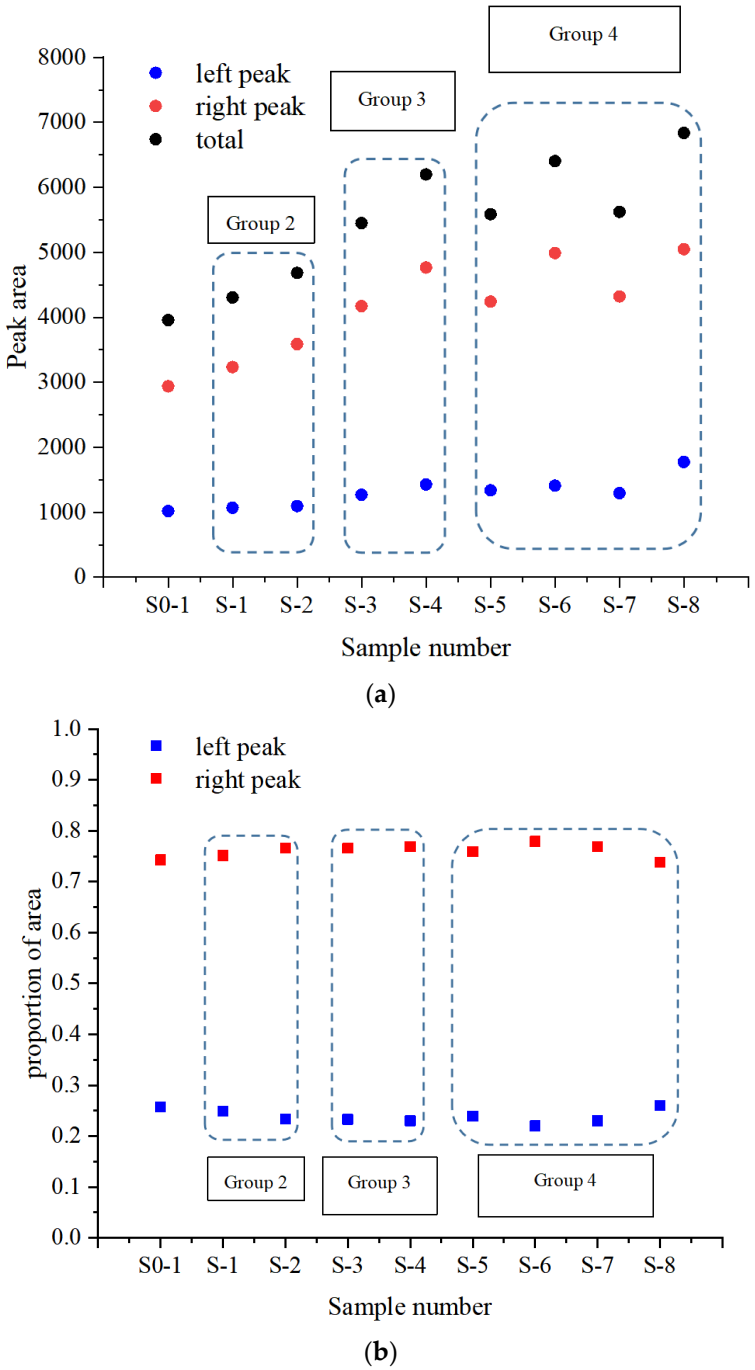

Figure 5. Left and right peak area in T_2 spectra of granite under different stimulation experiments: (**a**) Peak area of each sample; (**b**) Proportion of peak area.

Figure 5b shows that the ratio of the left and right peak area to the total spectra area of each sample is relatively stable, and macro-pores/micro-fractures always dominate. Among them, the proportion of the left peak area of each sample is between 0.23 and 0.26, and the proportion of the right peak area is between 0.74 and 0.77, which indicates that the increase of the pore-fracture space in the granite is dominated by macro-pores and micro-fractures conducive to fluid flow under the stimulation schemes of this experiment.

3.1.2. Variation of Porosity

Since the porosity of the three original samples is concentrated between 0.0078 and 0.0082, S0-1 is selected here as a representative sample and displayed in Figure 6 together with other treated samples. The porosities of samples S0-1, S-1 and S-2 in Figure 6 are 0.0081, 0.0094 and 0.011, respectively. It can be seen that the porosities of the samples after natural cooling at 300 °C and water cooling at 300 °C tend to increase, and the porosities of the granite samples after water cooling increase more than that of the granite after natural cooling.

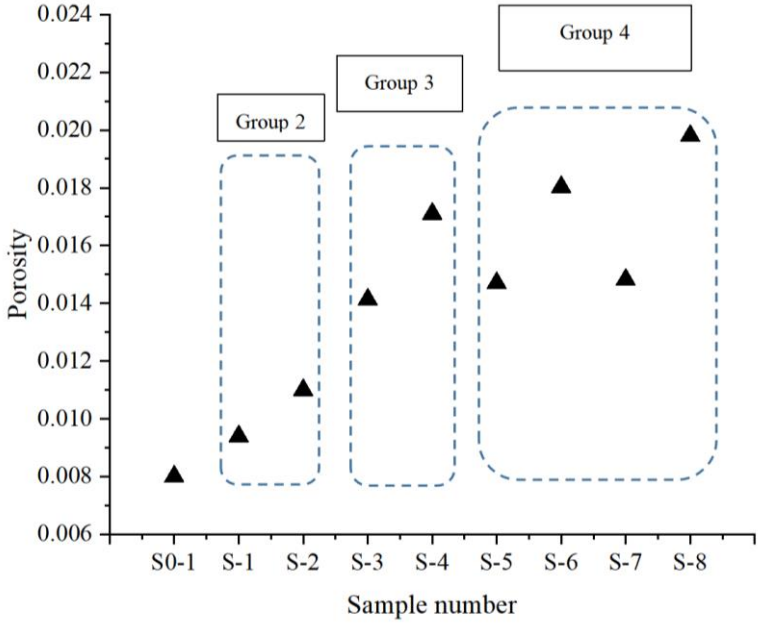

Figure 6. Porosity variation of granite under the action of different stimulation.

Comparing samples S0-1, S-3, S-5 and S-7, the porosities are 0.0081, 0.0142, 0.0147 and 0.0149, respectively. It can be seen that when the reaction time is 7 days, the porosity of granite increases significantly, and the effect of thermal-CO_2 superposition stimulation is more obvious.

The porosities of samples S-4, S-6 and S-8 are 0.0171, 0.0181 and 0.0198, respectively. Compared with S-3, S-5 and S-7, it is not difficult to see that when the reaction time increases from 7 d to 14 d, the porosities of granite samples further increased. There were significant differences between S-4, S-6 and S-8 in porosity. It indicates that the different heat treatment methods of the samples before the CO_2-water-rock reaction have a significant influence on the final stimulation effect. In conclusion, the scheme of water cooling after high temperature heating + high temperature and pressure CO_2-water-rock reaction had the most obvious stimulation effect, with the porosity increasing by 144.4%.

3.1.3. Variation of Permeability

The permeability of each sample was measured by the transient pulse method, and the results are shown in Figure 7. Since the permeability of the three original samples is

concentrated between 0.025 mD and 0.039 mD, S0-1 is selected here as a representative sample.

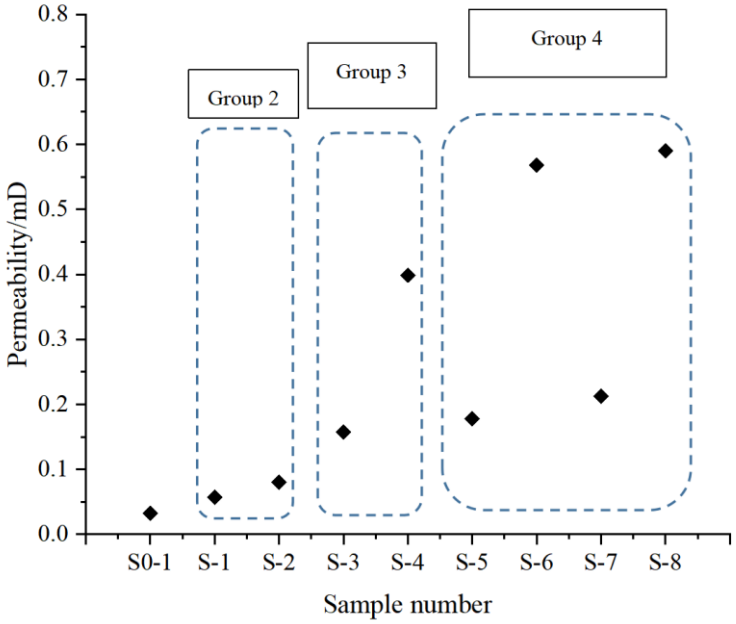

Figure 7. Permeability variation of granite under the action of different stimulation.

The permeability of samples S0-1, S-1 and S-2 is 0.032 mD, 0.057 mD and 0.081 mD, respectively. It can be seen that after being heated at 300 °C, the permeability of granite samples treated with natural cooling and water cooling have a tendency to increase, compared with the original samples, which are 179% and 250.68% of the original samples, respectively.

The permeability of samples S-3, S-5 and S-7 is 0.158 mD, 0.178 mD and 0.212 mD, respectively. Compared with sample S0-1, it is not difficult to find that the permeability of granite significantly increases after the high temperature and pressure CO_2-water-rock reaction for 7 days. The permeability of samples S-4, S-6 and S-8 is 0.399 mD, 0.568 mD and 0.591 mD, respectively. It indicates that different heat treatment methods before the reaction also have a slight effect on the change of permeability. The permeability of sample S-8 under the stimulation scheme of water cooling after high temperature heating + high temperature and high pressure CO_2-water-rock reaction is the largest, which is 1843.75% of the original.

3.1.4. Correlation Analysis between Porosity and Permeability

According to previous studies, the permeability of porous materials has a strong correlation with their micro-structure [55–61]. In this section, the permeability and porosity of granite samples after chemical-thermal stimulation can be fitted based on experiments. The porosity and permeability of each sample are plotted and fitted in Figure 8.

Equation (5) is obtained by fitting:

$$k = 7.95 \times 10^5 \phi^{3.6} \quad (5)$$

where k is permeability, mD; ϕ is porosity. $R^2 = 0.955$, indicating that the correlation is well fit by log-linear relation. It shows that the larger the porosity, the larger the pore space in the rock, and the larger the permeability of the sample. This indicates that there is a strong positive correlation between the porosity and the permeability of granite caused by different types of stimulation methods. The porosity of the granite subjected to combined stimulation is larger than that of the pure thermal or chemical stimulation, and its permeability is also larger. This also indicates that thermal/chemical stimulation causes new micro-fractures in

the granite sample or enhances the connectivity of the original pores. The sample S-8 under the stimulation scheme of water cooling after high temperature heating + high temperature and high pressure CO_2-water-rock reaction has the largest porosity and permeability.

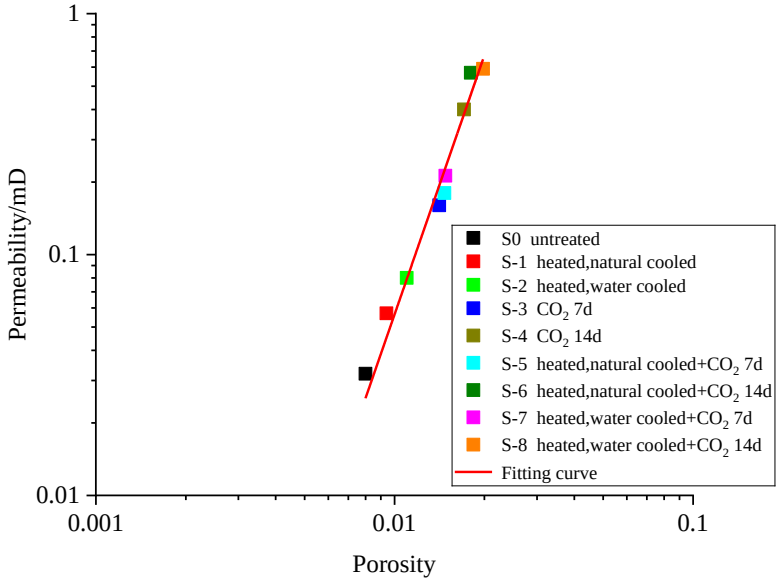

Figure 8. Relationship between permeability and porosity for granite after different types of stimulation.

3.2. Changes of Mechanical Properties of Granite

3.2.1. Stress-Strain Curves and Mechanical Parameters

Figure 9 shows the stress-strain curves of each granite sample under triaxial compression. In order to make the figure as easy to see as possible, only S0-1 in the original sample group is shown. The variation trend of the curves are very similar, indicating that the granite has good homogeneity. Under the confining pressure of 10 MPa, the brittle failure after the peak stress is obvious. The yield phase of the curve is very short, and the deviatoric stress falls quickly after reaching the peak strength.

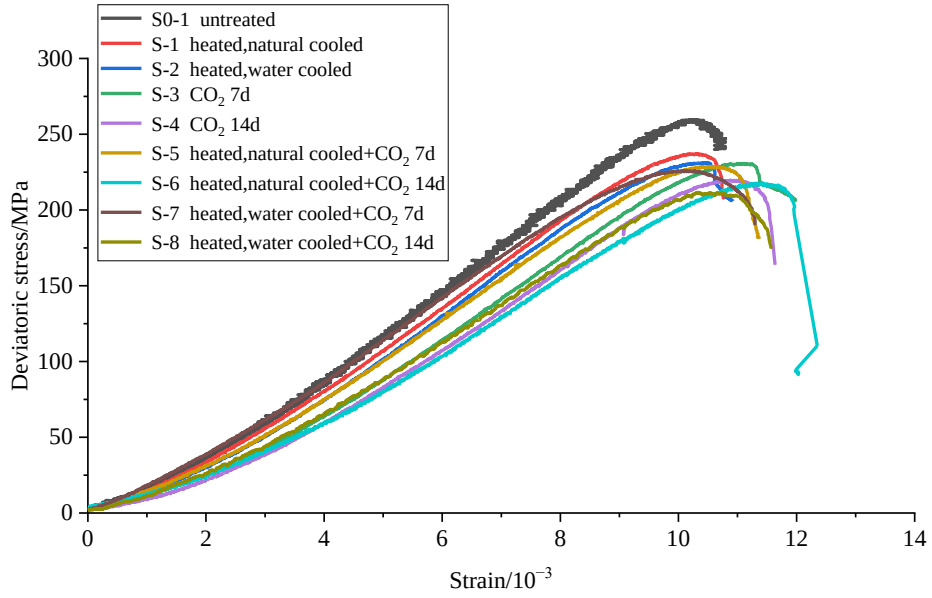

Figure 9. Deviatoric stress-axial strain curves of granite under different types of stimulation treatments.

The elastic modulus and peak strength of each granite sample are shown in Figure 10. Since the elastic modulus and strength of the original sample group are concentrated between 29.1~29.8 GPa and 251~256 MPa, respectively, we believe that S0-1 can be displayed as a representative sample. Comparing S0-1 with S-1 and S-2, it can be found that the elastic modulus and peak strength of granite decrease to a certain extent after heating at 300 °C. Additionally, the S-2 granite cooled in water has a higher degree of deterioration and a lower elastic modulus and peak strength than the S-1 granite after natural cooling.

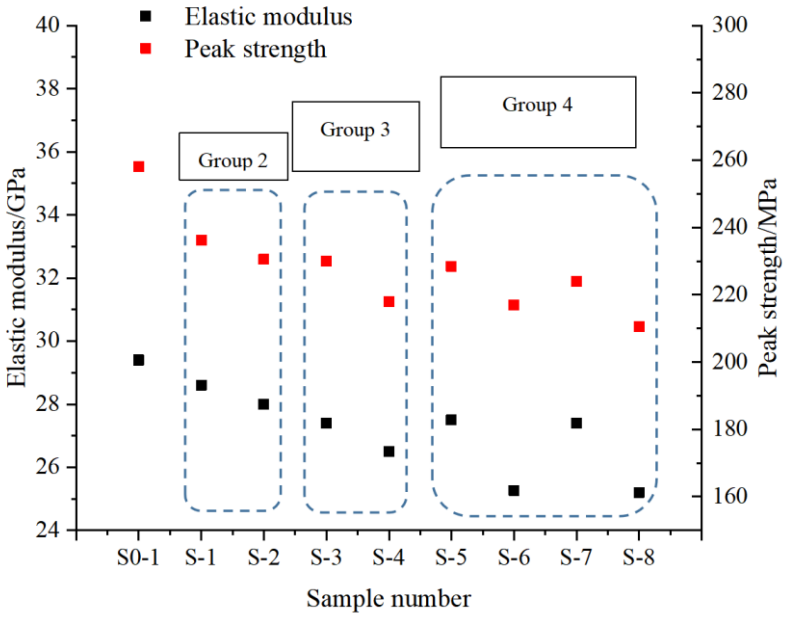

Figure 10. Elastic modulus and peak strength of granite under different types of stimulation treatment.

By comparing S0-1, S-3 and S-4, it can be found that the mechanical parameters of granite have obvious deterioration after CO_2-water-rock reaction at high temperature and pressure. When the reaction time corresponds to 7 d and 14 d, the elastic modulus decreases by 2 GPa and 2.9 GPa, and the peak strength decreases by 28 MPa and 40 MPa, respectively. By comparing S-3, S-5 and S-7, as well as S-4, S-6 and S-8, it shows that the thermal treatment of granite samples before CO_2-water-rock reaction leads to a higher degree of deterioration of mechanical parameters under the combined stimulation of water cooling, high temperature and pressure CO_2-water-rock reaction after high temperature heating treatment. The deterioration of elastic modulus and peak strength was the highest, which decreased by 14.3% and 18.41%, respectively.

3.2.2. Correlation Analysis between Porosity and Mechanical Parameters of Granite

According to previous studies, the micro-structure of granite has a significant influence on its mechanical properties [62]. By means of a nuclear magnetic resonance test, the relationship between the porosity and the mechanical parameters of the granite was studied [63]. In this paper, the linear correlation between the porosity and the elastic modulus and peak strength of the granite is also shown in Figure 11.

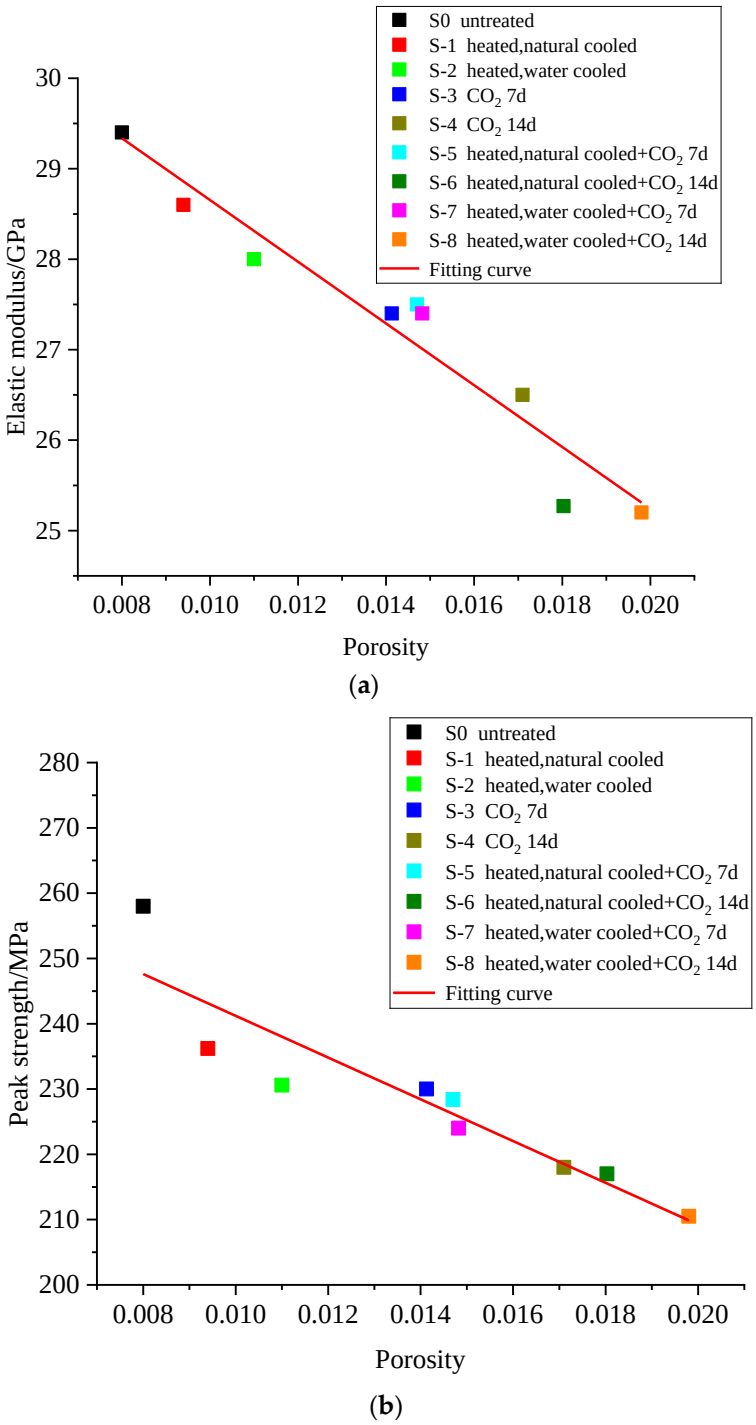

Figure 11. Relationship between mechanical parameters and porosity in granite samples after different types of treatment: (**a**) Elastic modulus; (**b**)compressive strength.

As can be seen in Figure 11, both the elastic modulus and compressive strength of granite have strong negative correlation with the porosity. The linear fitting relationship between porosity and these two mechanical parameters is as follows:

$$E = -341.2\phi + 32.06,\ R^2 = 0.934 \quad (6)$$

$$\sigma = -3197.25\phi + 273.2,\ R^2 = 0.852 \quad (7)$$

where E is the elastic modulus, GPa; σ is the compression strength, MPa.

The above equations show that the elastic modulus and compressive strength of rock decrease with the increase of pore volume, and the mechanical properties of granite deteriorate accordingly. The increase of pore volume mainly from micro-fractures is an important reason for the change of mechanical properties of granite after stimulation. The increase of rock pore volume reflects that some mineral particles are destroyed or dissolved under the combined thermal-chemical stimulation and the internal micro-fractures of granite increase, which makes the overall mechanical properties of the rock deteriorate. It is obvious that the combined stimulation scheme has a higher impact on pore volume and mechanical properties of granite; see Figure 11. After high temperature heating and water cooling, together with the CO_2-water-rock reaction at high temperature and pressure, the S-8 granite sample has the largest porosity and the highest deterioration degree of mechanical parameters.

3.2.3. Mechanism of Thermal Stimulation and CO_2 Bearing Solution Stimulation on Granite

According to the previous research results, due to the different thermal expansion coefficients of various mineral particles, when the rock is heated at a relatively high temperature, the deformation of mineral particles in the rock is inconsistent, resulting in thermal stress. When the thermal stress exceeds the particle bond strength, the particle bonding will be destroyed, causing new micro-cracks or further development of existing cracks [15,64,65]. When the granite samples with high temperature are rapidly cooled, a large temperature gradient occurs in the rocks, causing the non-uniform deformation in the rocks. The thermal stress is greater than the cohesion between mineral particles, and fractures occur [20,66].

CO_2 dissolved in water will lead to the dissolution of some minerals in granite. Since the solution containing CO_2 is weakly acidic, quartz (SiO_2) will dissolve with water:

$$SiO_2 + nH_2O \rightarrow SiO_2 \cdot nH_2O \quad (8)$$

At the same time, an acidic environment will lead to the hydrolysis of potassium feldspar ($KAlSi_3O_8$), albite ($NaAlSi_3O_8$) and other minerals:

$$2KAlSi_3O_8 + 2H^+ + 9H_2O \rightarrow Al_2Si_2O_5(OH)_4 + 2K^+ + 4H_4SiO_4 \quad (9)$$

$$2NaAlSi_3O_8 + 2CO_2 + 3H_2O \rightarrow Al_2Si_2O_5(OH)_4 + 2Na^+ + 4SiO_2 + 2HCO_3^- \quad (10)$$

The CO_2-water-rock reaction dissolves some minerals in the granite, causing the micro-pores or micro-fractures, which change the micro-structure of granite. Thus, it is beneficial for the fluid seepage due to the increase of porosity [34–39].

According to the micro-structure obtained by NMR analysis, it can be analyzed that the permeability and mechanical properties are closely related to the micro-structure of granite. Compared with the pure stimulation method, the combined thermal and CO_2 stimulation has a higher impact on the permeability and mechanical properties of granite, making the increases in the permeability and the deterioration of two mechanical parameters of elastic modulus and peak strength significant.

4. Conclusions

In this paper, the effects of different stimulation methods on the micro-structure, permeability and mechanical properties of granite were studied, involving the comparative experiments of thermal stimulation, CO_2 aqueous solution chemical stimulation and thermal stimulation combined with CO_2 bearing solution hydro-chemical stimulation at high temperature and high pressure. The main conclusions are as follows:

(1) Compared with the pure thermal or chemical stimulation, the superposition of thermal and CO_2 hydro-chemical solution stimulation has a more positive promotion effect on the development of micro-fractures in granite, which causes an increase

in permeability and a decrease in elastic modulus and compressive strength. When the granite is heated to 300 °C and subjected to water cooling and CO_2-water-rock reaction under high temperature and high pressure (240 °C, 20 MPa), the porosity increases by 27.6%, the permeability increases by 17 times, and the elastic modulus and peak strength degrade by 14.3% and 18.4%, respectively.

(2) There is a strong correlation between porosity, permeability, elastic modulus and compressive strength of granite before and after combined thermal and chemical stimulation. The elastic modulus and compressive strength are negatively correlated with the porosity.

(3) The combination of thermal and CO_2 bearing fluid hydro-chemical stimulation technology can result in the variation of micro-structures of granite, which is helpful to reduce the mechanical strength of granite especially adjacent to the wellbore region, decreasing the intensity of subsequent hydraulic fracturing or supercritical CO_2 fracturing.

Author Contributions: Conceptualization, R.-C.T. and H.-J.L.; methodology, R.-C.T. and H.-J.L.; software, R.-C.T.; validation, R.-C.T., H.-J.L. and Y.-J.S.; formal analysis, R.-C.T.; investigation, R.-C.T., H.-J.L., Y.-J.S., L.-H.X. and S.-N.B.; resources, H.-J.L. and Y.-J.S.; data collection, R.-C.T.; writing—original draft preparation, R.-C.T.; writing—review and editing, R.-C.T., H.-J.L., Y.-J.S., L.-H.X. and S.-N.B.; visualization, R.-C.T.; supervision, H.-J.L.; project administration, H.-J.L.; funding acquisition, H.-J.L. All authors have read and agreed to the published version of the manuscript.

Funding: This work was supported by the CAS Pioneer Hundred Talents Program (Y826031C01).

Data Availability Statement: The data presented in this study are available on request from the corresponding author.

Conflicts of Interest: The authors declare no conflict of interest.

References

1. Blackwell, D.; Frone, Z.; Richards, M. The future of geothermal energy: The shale gas analogy significant electrical EGS resource areas in the US. *Trans. Geotherm. Resour. Council.* **2013**, *37*, 117–122.
2. Liu, H.; Wang, H.; Lei, H.; Zhang, L.; Zhou, L. Numerical modeling of thermal breakthrough induced by geothermal production in fractured granite. *J. Rock Mech. Geotech. Eng.* **2020**, *12*, 900–916. [CrossRef]
3. Chen, S.; Ding, B.; Gong, L.; Huang, Z.; Yu, B.; Sun, S. Comparison of multi-field coupling numerical simulation in hot dry rock thermal exploitation of enhanced geothermal systems. *Adv. Geo-Energy Res.* **2019**, *3*, 396–409. [CrossRef]
4. Lin, P.; Ping, Z.; Lin, S.; Zhang, Z. Advances in research on reservoirs of enhanced geothermal system. *Sino-Glob. Energy* **2015**, *20*, 21–30.
5. Zhang, L.; Luo, F.; Xu, R.; Jiang, P.; Liu, H. Heat transfer and fluid transport of supercritical CO_2 in enhanced geothermal system with local thermal non-equilibrium model. *Energy Procedia* **2014**, *63*, 7644–7650. [CrossRef]
6. Evans, K.; Zappone, A.; Kraft, T.; Deichmann, N.; Moja, F. A survey of the induced seismic responses to fluid injection in geothermal and CO_2 reservoirs in Europe. *Geothermics* **2012**, *41*, 30–54. [CrossRef]
7. Li, H.; Jiang, X.; Xu, Z.; Bowden, S. The effect of supercritical CO_2 on failure mechanisms of hot dry rock. *Adv. Geo-Energy Res.* **2022**, *6*, 324–333. [CrossRef]
8. Davies, R.; Foulger, G.; Bindley, A.; Styles, P. Induced seismicity and hydraulic fracturing for the recovery of hydrocarbons. *Mar. Pet. Geol.* **2013**, *45*, 171–185. [CrossRef]
9. Rubinstein, J.L.; Mahani, A.B. Myths and facts on wastewater injection, hydraulic fracturing, enhanced oil recovery, and induced seismicity. *Seismol. Res. Lett.* **2015**, *86*, 1060–1067. [CrossRef]
10. Pearson, C. The relationship between microseismicity and high pore pressures during hydraulic stimulation experiments in low permeability granitic rocks. *J. Geophys. Res.* **1981**, *86*, 7855–7864. [CrossRef]
11. Jupe, A.J.; Green, A.; Wallroth, T. Induced microseismicity and reservoir growth at the Fjällbacka hot dry rocks project, Sweden. *Int. J. Rock Mech. Min. Sci. Geomech. Abstr.* **1992**, *29*, 343–354. [CrossRef]
12. Siratovich, P.A.; Sass, I.; Homuth, S.; Bjornsson, A. Thermal stimulation of geothermal reservoirs and laboratory investigation of thermally induced fractures. *Trans.-Geotherm. Resour. Council.* **2011**, *35*, 1529–1535.
13. Portier, S.; Vuataz, F.D.; Nami, P.; Sanjun, B.; Gérard, A. Chemical stimulation techniques for geothermal wells: Experiments on the 3-well EGS system at Soultz-sous-forets, France. *Geothermics* **2009**, *38*, 349–359. [CrossRef]

14. Zhou, Z.; Liu, S.; Liu, J. Study on the characteristics and development strategies of geothermal resources in China. *J. Nat. Resour.* **2015**, *30*, 1210–1221.
15. Chaki, S.; Takarali, M.; Agbodjan, W.P. Influence of thermal damage on physical properties of a granite rock: Porosity, permeability and ultrasonic wave evolutions. *Constr. Build. Mater.* **2007**, *22*, 1456–1461. [CrossRef]
16. Brace, W.F.; Walsh, J.B.; Frangos, W.T. Permeability of granite under high pressure. *J. Geophys. Res.* **1968**, *73*, 2225–2236. [CrossRef]
17. Alm, O.; Jaktlund, L. The influence of microcrack density on the elastic and fracture mechanical properties of Stripa granite Ove Aim and Lise-Lotte Jaktlund. *Phys. Earth Planet. Inter.* **1985**, *40*, 161–179. [CrossRef]
18. Kumari, W.G.P.; Ranjith, P.G.; Perera, M.S.A.; Chen, B.K.; Abdulagatov, I.W. Temperature-dependent mechanical behaviour of Australian Strathbogie granite with different cooling treatments-ScienceDirect. *Eng. Geol.* **2017**, *229*, 31–44. [CrossRef]
19. Brotóns, V.; Tomás, R.; Ivorra, S.; Alarcón, J.C. Temperature influence on the physical and mechanical properties of a porous rock: San Julian's calcarenite. *Eng. Geol.* **2013**, *167*, 117–127. [CrossRef]
20. Zhang, F.; Zhao, J.; Hu, D.; Skoczylas, F.; Shao, J. Laboratory investigation on physical and mechanical properties of granite after heating and water cooling treatment. *Rock Mech. Rock Eng.* **2018**, *51*, 677–694. [CrossRef]
21. Madirisha, M.; Hack, R.; Meer, F. The influence of chelating agents on clays in geothermal reservoir formations: Implications to reservoir acid stimulation. *Geothermics* **2022**, *99*, 102305. [CrossRef]
22. Xu, T.; Rose, P.; Fayer, S.; Pruess, K. On modeling of chemical stimulation of an enhanced geothermal system using a high pH solution with chelating agent. *Geofluids* **2009**, *9*, 167–177. [CrossRef]
23. Portier, S.; André, L.; Vuataz, F.D. Review on chemical stimulation techniques in oil industry and applications to geothermal systems. *Engineering* **2007**, *32*, 1–30.
24. Xu, J.; Feng, B.; Cui, Z.; Liu, X.; Ke, Z.; Feng, G. Comparative study of acid and alkaline stimulants with granite in an enhanced geothermal system. *Acta Geol. Sin. (Engl. Ed.)* **2021**, *95*, 1926–1939. [CrossRef]
25. Na, J.; Xu, T.; Wu, Y.; Feng, B.; Bao, X. Effectiveness of using mud acid as stimulation agent for enhanced geothermal systems (EGS) reservoir. *J. Cent. South Univ. (Sci. Technol.)* **2017**, *48*, 247–254.
26. Wakahama, H.; Mitoa, S.; Ohsumi, T.; Ueda, A.; Yajima, T.; Satoh, H.; Sugiyama, K.; Ozawa, A.; Ajima, S.; Todaka, N. A concept of CO_2 georeactor sequestration at the Ogachi HDR site, NE Japan. *Energy Procedia* **2009**, *1*, 3683–3689. [CrossRef]
27. Matthes, L.; Lummer, R. Next generation acids-new retarded system for geothermal applications. *Erdol Erdgas Kohle* **2014**, *130*, 39–40.
28. Qu, X.; Liu, L.; Ma, R.; Hu, D.; Chen, X.; Wang, Y. Experiment on debris-arkosic sandstone reformation by CO_2 fluid. *J. Jilin Univ. (Earth Sci. Ed.)* **2008**, *38*, 959–964.
29. Wang, G.; Zhao, J.; Zhang, F.; Tao, Y.; Yang, X.; Wang, H. Interactions of CO_2-brine-rock in sandstone reservoir. *J. Cent. South Univ. (Sci. Technol.)* **2013**, *44*, 1168–1173.
30. Ma, D.; Chen, Q.; Zhou, H.; Teng, Q.; Li, K.; Hu, D. Experimental study of liquid CO_2 fracturing mechanism of glutenite. *Rock Soil Mech.* **2020**, *41*, 3996–4004.
31. Zhao, R.; Sun, H.; Wu, Y.; Zhao, C. Influence of CO_2 corrosion on rock structure and its mechanical characteristics. *Sci. China Technol. Sci.* **2010**, *40*, 822–828. [CrossRef]
32. Liu, H.; Shi, Y.; Fang, Z.; Liu, J.; Tong, R. Seepage characteristics of thermally and chemically treated Mesozoic granite from geothermal region of Liaodong Peninsula. *Environ. Earth Sci.* **2021**, *80*, 599. [CrossRef]
33. Miao, S.; Cai, M.; Guo, Q.; Wang, P.; Liang, M. Damage effects and mechanisms in granite treated with acidic chemical solutions. *Int. J. Rock Mech. Min. Sci.* **2016**, *88*, 77–86. [CrossRef]
34. Xu, T.; Wang, W.; Pruess, K. *Numerical Simulation to Study the Feasibility of Using CO_2 as a Stimulation Agent for Enhanced Geothermal Systems*; Lawrence Berkeley National Lab.: Berkeley, CA, USA, 2010; pp. 1–8.
35. Rosenbauer, R.J.; Koksalan, T.; Palandri, J.L. Experimental investigation of CO_2-brine-rock interactions at elevated temperature and pressure: Implications for CO_2 sequestration in deep-saline aquifers. *Fuel Process. Technol.* **2005**, *8*, 1581–1597. [CrossRef]
36. Suto, Y.; Liu, L.; Yamasaki, N.; Hashidal, T. Initial behavior of granite in response to injection of CO_2-saturated fluid. *Appl. Geochem.* **2007**, *22*, 202–218. [CrossRef]
37. Shao, H.; Thompson, C.J.; Cantrell, K.J. Evaluation of experimentally measured and model-calculated pH for rock-brine-CO_2 systems under geologic CO_2 sequestration conditions. *Chem. Geology.* **2013**, *359*, 116–124. [CrossRef]
38. Zheng, L.; Spycher, N.; Birkholzer, J.; Xu, T.; Apps, J.; Kharaka, Y. On modeling the potential impacts of CO_2 sequestration on shallow groundwater: Transport of organics and co-injected H_2S by supercritical CO_2 to shallow aquifers. *Int. J. Greenh. Gas Control* **2013**, *14*, 113–127. [CrossRef]
39. Ré, C.L.; Kaszuba, J.P.; Moore, J.N.; McPhersonc, B.J. Fluid-rock interactions in CO_2-saturated, granite-hosted geothermal systems: Implications for natural and engineered systems from geochemical experiments and models. *Geochim. Et Cosmochim. Acta.* **2014**, *141*, 160–178.
40. Shiraki, R.; Dunn, T.L. Experimental study on water-rock interactions during CO_2 flooding in the Tensleep Formation, Wyoming, USA. *Appl. Geochem.* **2000**, *15*, 265–279. [CrossRef]
41. Isaka, B.L.A.; Ranjith, P.G.; Rathnaweera, T.D.; Perera, M.S.A.; Kumari, W.G.P. Influence of long-term operation of supercritical carbon dioxide based enhanced geothermal system on mineralogical and microstructurally-induced mechanical alteration of surrounding rock mass. *Renew. Energy* **2019**, *136*, 428–441. [CrossRef]

42. Zhou, K.; Li, J.; Xu, Y.; Zhang, Y.; Yang, P.; Chen, L. Experimental study of NMR characteristics in rock under freezing and thawing cycles. *Chin. J. Rock Mech. Eng.* **2012**, *31*, 731–737.
43. Williams, J.L.A.; Taylor, D.G.; Maddinelli, G.; Enwere, P.; Archer, J.S. Visualization of fluid displacement in rock cores by NMR imaging. *Magn. Reson. Imaging* **1991**, *9*, 767–773. [CrossRef]
44. Lucas-Oliveira, E.; Araujo-Ferreira, A.G.; Trevizan, W.A.; DosSantos, B.C.; Bonagamba, T.J. Sandstone surface relaxivity determined by NMR T_2 distribution and digital rock simulation for permeability evaluation. *J. Pet. Sci. Eng.* **2020**, *193*, 107400. [CrossRef]
45. Zhao, D.; Yuan, P. Research on the influence rule of ultrasonic vibration time on granite damage. *J. Min. Sci.* **2018**, *54*, 751–762. [CrossRef]
46. Nakashima, Y.; Nakano, T.; Nakamura, K.; Uesugi, K.; Tsuchiyama, A.; Ikeda, S. Three-dimensional diffusion of non-sorbing species in porous sandstone: Computer simulation based on X-ray micro-tomography using synchrotron radiation. *J. Contam. Hydrol.* **2004**, *74*, 253–264. [CrossRef]
47. Yao, Y.; Liu, D.; Yao, C.; Tang, D.; Tang, S.; Huang, W. Petrophysical characterization of coals by low-field nuclear magnetic resonance (NMR). *Fuel* **2010**, *89*, 1371–1380. [CrossRef]
48. Liu, J.; Jiang, X.; Huang, X.; Wu, S. Morphological characterization of super fine pulverized coal particle. Part 2. AFM investigation of single coal particle. *Fuel* **2010**, *89*, 3884–3891. [CrossRef]
49. Wang, H.; Yu, L.; Song, Y.; Zhao, Y.; Zhao, J.; Wang, D. Fractal analysis and its impact factors on pore structure of artificial cores based on the images obtained using magnetic resonance imaging. *J. Appl. Geophys.* **2012**, *86*, 70–81. [CrossRef]
50. Guo, C.; Qin, Y.; Ma, D.; Xia, Y.; Bao, Y.; Chen, Y.; Lu, L. Pore structure and permeability characterization of high-rank coal reservoirs: A case of the Bide-Santang basin, Western Guizhou, South China. *Acta Geol. Sin. (Engl. Ed.)* **2020**, *94*, 29–38. [CrossRef]
51. Cai, Y.; Liu, D.; Pan, Z.; Yao, Y.; Li, J.; Qiu, Y. Pore structure and its impact on CH_4 adsorption capacity and flow capability of bituminous and sub-bituminous coals from Northeast China. *Fuel* **2013**, *103*, 258–268. [CrossRef]
52. Cai, Y.; Liu, D.; Pan, Z.; Che, Y.; Liu, Z. Investigating the effects of seepage-pores and fractures on coal permeability by fractal analysis. *Transp. Porous Media.* **2016**, *111*, 479–497. [CrossRef]
53. Li, Q.; Li, X.; Yin, T. Factors affecting pore structure of granite under cyclic heating and cooling: A nuclear magnetic resonance investigation. *Geothermics* **2021**, *96*, 102198. [CrossRef]
54. Chen, S.; Tang, D.; Tao, S.; Ji, X.; Xu, H. Fractal analysis of the dynamic variation in pore-fracture systems under the action of stress using a low-field NMR relaxation method: An experimental study of coals from western Guizhou in China. *J. Pet. Sci. Eng.* **2019**, *173*, 617–629. [CrossRef]
55. Kozeny, J. Ueber die kapillare Leitung des Wassers im Boden. *Stizungsber Akad Wiss Wien.* **1927**, *136*, 271–306.
56. Carman, P.C. Fluid flow through granular beds. *Trans. Inst. Chem. Eng.* **1973**, *15*, 150–167. [CrossRef]
57. Na, J.; Feng, B.; Lan, C.; Xu, T.; Bao, X. Effectiveness of using supercritical CO_2 as stimulation agent for enhanced geothermal systems. *J. Cent. South Univ. (Sci. Technol.)* **2014**, *45*, 2447–2458.
58. Deng, S.; Jiang, Q.; Shang, K.; Jing, X.; Xiong, F. Effect of high temperature on micro-structure and permeability of granite. *Rock Soil Mech.* **2021**, *42*, 1601–1611.
59. Song, R.; Wang, Y.; Tang, Y.; Peng, J.; Liu, J.; Yang, C. 3D Printing of natural sandstone at pore scale and comparative analysis on micro-structure and single/two-phase flow properties. *Energy* **2022**, *261*, 125226. [CrossRef]
60. Song, R.; Liu, J.; Yang, C.; Sun, S. Study on the multi-phase heat and mass transfer mechanism in the dissociation of methane hydrate in reconstructed real-shape porous sediments. *Energy* **2022**, *254*, 124421. [CrossRef]
61. Neumann, M.; Stenzel, O.; Willot, F.; Holzer, L.; Schmidt, V. Quantifying the influence of microstructure on effective conductivity and permeability: Virtual materials testing. *Int. J. Solids Struct.* **2020**, *184*, 211–220. [CrossRef]
62. Ge, X.; Xiao, Y.; Fan, Y.; Liu, J.; Zhang, Y. Laboratory investigation of the relationship between static rock elastic parameters and low field nuclear magnetic resonance data. *Int. J. Rock Mech. Min. Sci.* **2020**, *127*, 104207. [CrossRef]
63. Siratovich, P.A.; Villeneuve, M.C.; Cole, J.W.; Kennedy, B.M.; Bégué, F. Saturated heating and quenching of three crustal rocks and implications for thermal stimulation of permeability in geothermal reservoirs-ScienceDirect. *Int. J. Rock Mech. Min. Sci.* **2015**, *80*, 265–280. [CrossRef]
64. Xi, B.; Cheng, Z.; He, S.; Yang, Y.; Liu, J. Experimental study on permeability characteristics and its evolution of granite after high temperature. *Chin. J. Rock Mech. Eng.* **2021**, *40*, 2716–2723.
65. Kovacik, J. Correlation between Young's modulus and porosity in porous materials. *J. Mater. Sci. Lett.* **1999**, *18*, 1007–1010. [CrossRef]
66. Cheng, Z.; Xi, B.; Yang, X.; He, S.; Li, X. Experimental study on the evolution of granite permeability under thermal shock. *J. Taiyuan Univ. Technol.* **2021**, *52*, 198–203.